Contrib Mineral Petrol (1994) 117:394–409

Cuneyt Sen · Todd Dunn

Dehydration melting of a basaltic composition amphibolite at 1.5 and 2.0 GPa: implications for the origin of adakites

Received: 21 October 1993 / Accepted: 25 March 1994

Abstract This study presents the results of dehydration melting experiments on a basaltic composition amphibolite under conditions appropriate to a hot slab geotherm (1.5 and 2.0 GPa and temperatures of 850 to 1150° C). Dehydration melting produces an omphacitic augite and garnet bearing residue coexisting with rhyolitic to andesitic composition melts. At 1.5 GPa, the amphibolite melts in two stages between 800 and 1025° C. The 2.0 GPa data also define two melting stages. At 2.0 GPa, the first stage involves nearly modal melting of the original amphibolite minerals (qtz, pl, amp) to produce melt + cpx + grt. During the second stage, the eclogite restite melts non-modally (0.86 cpx + 0.14 grt = 1 melt). The experimental results were combined with data from the literature to generate a composite *P-T* phase diagram for basaltic composition amphibolites over the 800 to 1100° C temperature range for pressures up to 2.0 GPa. Comparison of the major element compositions of the experimentally produced melts with compositions of presumed slab melts (adakites) shows that partial melting of amphibolite at conditions appropriate to a hot-slab geotherm produces melts similar to andesitic and dacitic adakites except for significant MgO and CaO depletions. Trace element modelling of amphibolite dehydration melting using the 2.0 GPa melting reactions produces REE abundances similar to those of adakites at 10–15 wt% batch melting, but the models do not reproduce the high Sr/Y ratios characteristic of adakites. Taken together, the major and trace element results are not consistent with the derivation of adakites by dehydration melting of the subducted slab with little or no interaction with the mantle wedge or crust. If adakites are partial melts of the subducted slab, they must undergo significant interaction with the mantle and/or crust, during which they acquire a number of their distinctive characteristics.

C. Sen[1] · T. Dunn (✉)
Department of Geology, University of New Brunswick, Fredericton, N.B. E3B 5A3, Canada

[1] *Present address:*
Jeoloji Bölümü; Karadeniz Teknik Üniversitesi, Trabzon, Turkey 61015

Editorial responsibility: T. Grove

Introduction

During subduction the oceanic crust undergoes progressive metamorphism from greenschist to amphibolite and finally to the eclogite facies. The facies changes are accompanied by progressive release of fluids from the slab. The depths at which the greenschist to amphibolite and amphibolite to eclogite transitions occur are dependent on the thermal state of the slab at the onset of subduction (Peacock 1991, 1993). If the subducted slab is relatively young and hot at the point of subduction, it will have a steeper dT/dP slope than a colder slab and will be correspondingly hotter at any given depth (Fig. 1). In the extreme case, the slab geotherm may intersect the amphibolite dehydration melting solidus and the slab may partially melt. Partial melts of the subducted slab are thought to be hydrous silicic melts (Rapp et al. 1991), which may rise into and modally metasomatize the overlying mantle wedge peridotites (e.g., Nicholls and Ringwood 1973; Sekine and Wyllie 1982; Johnston and Wyllie 1989), or they may pass through the mantle wedge and be emplaced in the crust or erupted onto the surface (i.e., adakites; Defant and Drummond 1990, 1993; Defant et al. 1991). Consequently, knowledge of the melting relations of amphibolite facies metabasites and the major and trace element compositions of the partial melts is required in order to understand more fully the modal metasomatism of the mantle wedge and the origins of the presumed slab melts called adakites by Defant and Drummond (1990). While several workers have studied

the dehydration melting relations of natural amphibolites at crustal conditions (Beard and Lofgren 1991; Rushmer 1991; Wolf 1992), only Rapp et al. (1991) studied the melting relations of natural amphibolites at conditions appropriate to the hot slab geotherm (Fig. 1). However, while Rapp et al. (1991) presented partial melt compositions for a wide range of conditions, they did not determine melting relations, which are required for trace element modelling of melting.

This study presents the results of an experimental study of the melting relations of an amphibolite facies metabasite. Experiments were conducted at pressures of 1.5 and 2.0 GPa and temperatures of 800 to 1150° C, corresponding to the conditions at which the subducted slab starts to melt in the hot slab model (Peacock 1991, 1993). The major goals of the this study were to determine the phase changes that occur during dehydration melting of natural amphibolite, and to examine the effects of temperature and pressure on product minerals and melts. The results of this study are compared with data on presumed natural slab melts (adakites) in order to place further constraints on their origins. Trace element models, based on the derived amphibolite melting relations, are used to test the hypothesis that adakites are slab melts and to provide constraints on the trace element composition of the presumed slab sources of adakites. The melt compositions (both major and trace element) also provide the basis for modelling modal metasomatism of the mantle wedge (e.g., Sen 1994).

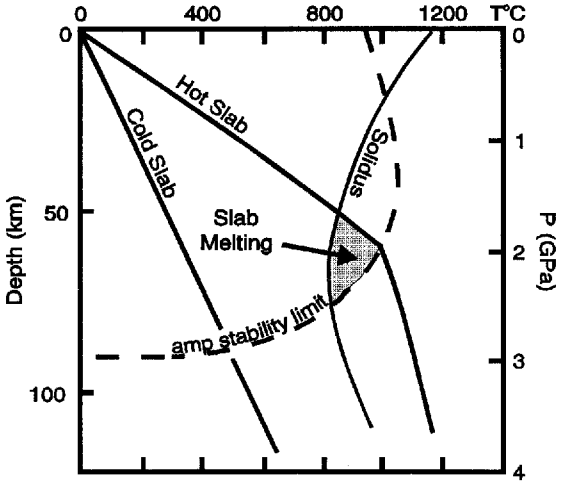

Fig. 1 Idealized *P-T* diagram showing hot and cold slab geotherms in subduction zones (adapted from Peacock 1991, 1993). The effective dehydration melting solidus for basaltic composition amphibolite is shown along with the approximate stability limit of amphibole in basaltic amphibolite. The *shaded area* shows the region of potential slab melting

Starting material

The starting material was an amphibolite from British Columbia, Canada. Bulk rock chemistry and average mineral analyses are given in Table 1. The mode was determined both by mass balance and point counting. The bulk composition of the starting amphibolite was determined by wavelength dispersive XRF and mineral compositions were determined by electron microprobe as described below. The mineral assemblage consists of ferroan pargasitic hornblende (76.3 wt%), An_{55} plagioclase (20.5 wt%), quartz (2.3 wt%), titanite (0.9 wt%) and garnet (< 0.1 wt%).

Sample preparation for the experiments consisted of crushing approximately 500 g of rock in a steel mortar and subsequently hand grinding with an agate mortar and pestle. The melting relations were investigated in preliminary experiments (24 h duration) using coarse (− 60/ + 120 mesh) splits. The same amount of rock sample, crushed to a fine powder (− 120 mesh) in a WC shatter box, was used as the starting material for the longer experiments.

Experimental and analytical procedures

All experiments (except D28 and D30, which were done in an end-loaded piston-cylinder apparatus, using the hot piston-out

Table 1 Compositions of the starting amphibolite and its constituent minerals. Average N-MORB is also shown for comparison. Numbers in brackets are the one sigma standard deviations of the averages in units of the least significant figure reported (*n.a.* not analyzed, *n.d.* not detected)

Phase	WR	Amp	Pl	Grt	Ttn	N-MORB[a]
n	3	15	7	6	5	
SiO_2	46.88(42)	42.54(28)	54.38(12)	38.28(16)	28.80(23)	50.45
TiO_2	1.22(1)	1.45(5)	n.d.	n.d.	38.98(17)	1.62
Al_2O_3	15.00(10)	12.11(35)	28.02(24)	21.48(14)	1.22(25)	15.26
MgO	8.25(5)	10.66(24)	n.d.)	4.46(14)	n.d.	7.58
CaO	11.28(7)	11.40(11)	10.58(8)	10.53(15)	27.80(35)	11.30
MnO	0.26(2)	0.23(11)	n.d.	2.74(9)	n.d.	–
FeO	8.70(14)[b]	11.50(20)[b]	0.16(3)	23.10(35)	0.81(11)	10.43
Fe_2O_3	4.88(14)[b]	4.28(30)[b]	n.a.	n.a.	n.a.	–
Na_2O	2.51(13)	1.54(10)	5.63(11)	n.d.	n.d.	2.68
K_2O	0.80(3)	0.77(5)	0.14(5)	n.d.	n.d.	0.11
H_2O	1.5(1)[c]	n.a.	n.a.	n.a.	n.a.	
Total	99.78[d]	96.48	99.09	100.59	97.61	

[a] Average N-MORB composition from Hofmann (1988)
[b] FeO was determined by titration. Fe_2O_3 was determined by difference between total iron and measured FeO
[c] H_2O was determined by infrared spectroscopy on a split of whole rock fused at 1300 °C and 1.5 GPa
[d] Anhydrous total

method, at the California Institute of Technology) were done in a non-end-loaded piston-cylinder apparatus, using the hot piston-in method, at the University of New Brunswick. All experiments were done in 1.27 cm diameter NaCl/Pyrex/crushable MgO sample assemblies. All but two experiments (M5 and B17, Table 2, which were done in Au capsules) were done in graphite lined Pt capsules. Sample capsules were loaded with 15 to 20 mg of sample, dried for at least 2 h at 110° C and then welded shut. Experiments designated "M" in Table 2 differ from normal experiments. The starting materials for those runs consisted of a layer of amphibolite and a layer of a model peridotite directly on top of the amphibolite. Temperature was measured with a $Pt_{87}Rh_{13}$-Pt thermocouple separated from the top of the sample capsule by a 0.5 mm thick alumina spacer. Power consumption was monitored during all runs in order to detect thermocouple drift. After initial stabilization, which occured in 2 to 3 h, no significant power drift was observed in any of the runs. Pressure was monitored with a Bourdon tube gauge and the reported pressures are thought to be accurate to within $\pm$ 0.05 GPa based on determinations of the melting point of NaCl at 1.5 GPa. After the experiments, the samples were cast in epoxy and sectioned vertically. A slice from the center of the charge was used to prepare a polished thin section which was examined by backscattered electron imaging and X-ray microanalysis.

Electron imaging and X-ray analysis were done at the University of New Brunswick, using a JEOL JSM-6400 scanning electron microscope equipped with a Link eXL energy dispersive analyzer and a single wavelength dispersive channel. X-ray analyses were carried out at an accelerating potential of 15 kV and a sample current of 2.5 nA, using a live time of 100 s for energy dispersive data acquisition. All elements were determined by the energy dispersive method except Na, which was determined by simultaneous wavelength dispersive analysis. The raw data were merged prior to ZAF correction. Standards used were: albite - Na, periclase - Mg, corundum - Al, wollastonite- Si, Ca, orthoclase - K and metals - Cr, Mn, Fe, Ti and Ni.

Alkali mobility in glasses, as a result of electron bombardment, is a complicating factor in X-ray analysis of hydrous silicate glasses. In order to minimize such effects and compensate for apparent alkali loss, a modified Beard and Lofgren (1991) approach was used. The electron beam was rastered over as large an area as possible (raster areas up to 20×20 microns were used, but were generally smaller due to the small sizes of the glass pools) to minimize sample heating. For each sample a representative melt pool was analyzed as follows. The wavelength dispersive spectrometer was set to the peak position for Na and repeated 2 s counts were collected over a total time of 80 s. The data were used to generate an Na-decay curve, which was used to extrapolate the count rate back to zero time. The Na loss in analyzed melt pools ranged from 5 to 10%. In actual analyses, Na was counted for only 20 s in an attempt to minimize the magnitude of this correction. Any remaining deficiency in the analysis totals is assumed to be due to H_2O and CO_2 dissolved in the melts (melts produced in the gold capsule experiments contain only H_2O).

The modes of the product phases in the experimental charges were determined by a combination of digital image analysis of backscattered electron images and mass balance calculations. For each sample, more than 25 random areas (150×110 μm) were scanned for image analysis. Amphibole and clinopyroxene were indistinguishable in backscattered electron images, because of their very similar mean atomic numbers. Therefore, modes were also calculated by mass balance using the chemical compositions of the phases. The garnet modes, determined by both methods were compared. Very similar results were obtained if the experimental charge consisted of four or fewer phases, but the uncertainty increased with increasing number of phases in the system. Modal abundances and uncertainties are reported in Table 2.

In order to determine approximately the oxygen fugacity in the Pt-C capsules, a sample of starting amphibolite was completely melted (1300° C, 1.5 GPa, 2 h) and the Fe^{2+}/Fe^{3+} ratio of the quenched glass was determined by titration. The oxygen fugacity was calculated from the ferric/ferrous ratio, melt composition, temperature and pressure with the equation of Kress and Carmichael (1991). The result, 0.5 $\log_{10}$ units below the fayalite-magnetite-quartz buffer, agrees well with the range of oxygen fugacities reported for mantle xenoliths collected from the subduction environment (e.g., Haggerty 1990). The dissolved H_2O and CO_2 in the melt were determined by infrared spectroscopy (Stolper 1982; Stolper and Holloway 1988) and found to be 1.5 $\pm$ 0.1 and 0.315 $\pm$ 0.015 wt%, respectively. The measured CO_2 value is consistent with the amount predicted by the Holloway et al. (1992) relationship among T, P, oxygen fugacity and the initial redox state of the sample. The water content of the sample is reasonable given the mode (Table 1) and expected water content of the amphibole, the only hydrous phase in the starting material. It appears that there was little reaction between water and carbon dioxide to form CO, CH_4 or H_2.

Table 2 Run conditions and phase proportions (wt %) from amphibolite melting experiments. Numbers in brackets are the one sigma standard deviations of the averages expressed in units of the least significant figure reported

Run	T°C	P(GPa)	t(h)	Cap[a]	Melt	Amp	Pl	Qtz	Grt	Cpx	Rt
B7	850	1.5	168	Pt-C	<0.1(1)	76.3(8)	20.5(5)	2.3(1)	<0.1(1)	–	tr
B1	875	1.5	24	Pt-C	<0.1(1)	76.3(8)	20.5(5)	2.3(1)	<0.1(1)	–	tr
B2	900	1.5	24	Pt-C	<0.1(1)	76.3(8)	20.5(5)	2.3(1)	<0.1(1)	<0.1(1)	tr
B3	925	1.5	24	Pt-C	1.0(5)	76.0(8)	20.0(5)	2.0(3)	1.0(5)	1.0(5)	tr
B18	925	1.5	120	Pt-C	1.9(5)	66.5(12)	16.3(20)	1.7(2)	5.0(25)	8.3(45)	tr
B4	950	1.5	24	Pt-C	14.6(30)	46.0(28)	14.5(18)	–	12.8(18)	6.0(36)	tr
M4	950	1.5	216	Pt-C	9.3(20)	54.3(50)	13.9(32)	–	9.2(18)	13.3(32)	tr
M5	950	1.5	144	Au	9.0(18)	58.1(38)	14.0(23)	–	6.3(20)	12.7(28)	tr
B5	975	1.5	24	Pt-C	19.4(25)	36.9(45)	8.6(12)	–	16.8(22)	10.9(24)	tr
M2	975	1.5	96	Pt-C	12.2(22)	38.6(72)	8.6(18)	–	19.2(20)	21.3(28)	tr
M14	1025	1.5	72	Pt-C	22.7(8)	6.1(18)	–	–	28.5(18)	42.7(18)	tr
B17	1025	1.5	120	Au	19.7(15)	20.4(26)	–	–	22.7(15)	37.2(24)	tr
D30	800	2.0	168	Pt-C	<0.1(1)	76.3(8)	20.5(5)	2.3(1)	<0.1(1)	<0.1(1)	tr
B8[b]	900	2.0	192	Pt-C	11.4(10)	8.6(20)	–	–	35.0(8)	38.4(12)	tr
B16	950	2.0	192	Pt-C	15.4(8)	–	–	–	38.4(10)	46.2(8)	tr
M6	975	2.0	96	Pt-C	16.4(10)	–	–	–	39.0(12)	40.5(8)	tr
B9	1025	2.0	96	Pt-C	20.6(10)	–	–	–	38.9(8)	40.4(12)	tr
D28	1150	2.0	48	Pt-C	24.6(10)	–	–	–	37.1(10)	38.3(10)	tr

[a] Capsules were either gold (Au) or graphite lined platinum (Pt-C)
[b] Run B8 also contained 3.8(2) % K-feldspar and 3.4(10) % biotite

No attempt was made to determine the oxygen fugacity in the Au capsule experiments. However, most previous studies of amphibolite dehydration melting (e.g., Beard and Lofgren 1991; Rapp et al. 1991; Rushmer 1991; Wolf 1992) estimated the oxygen fugacity in Au capsule runs to be somewhere between the hematite-magnetite and fayalite-magnetite-quartz buffers (commonly near Ni-NiO).

Approach to equilibrium

Beard and Lofgren (1991) are the only workers to have reversed vapor absent partial melting experiments on amphibolites. Their results demonstrated that isothermal runs of 96 h duration were sufficient to produce a reasonable approach to equilibrium melts and mineral assemblages at temperatures as low as to 900° C. The durations of our runs used to determine melting relationships ranged from 168 h at 800° C to 48 h at 1150° C. Intermediate temperature runs ranged between 72 and 216 h and all runs at temperatures below 1025° C were at least 96 h long (Table 2). As discussed below, garnets and clinopyroxenes produced in runs below 900° C were significantly heterogeneous. Thus, those runs did not achieve a close approach to equilibrium. However, the minerals in our higher temperature runs ($T \geqq 900°$ C) were reasonably homogeneous (Table 3). Since those runs were as long or longer than the times found to provide a reasonable approach to equilibrium by Beard and Lofgren (1991), we conclude that our longer runs at temperatures of 900° C and above were acceptably close to equilibrium.

Results

Phase modes

Figure 2 shows plots of the experimentally determined phase abundances (Table 2) versus temperature. Figure 2a and b shows the phase proportions produced in the short (24 h) and long (> 24 h) duration experiments done at 1.5 GPa, respectively. The results of run B14 (1025° C, 72 h, Table 2) are excluded from Fig. 2b, because comparison of the results of that run with those of run B-17 (1025° C, 120 h, Table 2) suggests that run B-14 lost water. The results of both sets of experiments are qualitatively similar, but the absolute abundances of the phases differ slightly. Based on the assumption that the longer experiments approached equilibrium more closely, those results are used to define the temperatures at which phases first occur and/or are completely consumed. While trace amounts of melt are present in all runs, significant melting does not begin until approximately 900° C. The onset of significant melting is coincident with the appearance of clinopyroxene and product garnet and the beginning of decreases in the abundances of amphibole, plagioclase and quartz (Fig. 2b). Furthermore, as discussed below, the melts present in runs done below 900° C are physically localized, heterogeneous in composition, and do not appear to be interconnected. Therefore, the effective solidus of the amphibolite is taken to be approximately 900° C at 1.5 GPa. Both plagioclase and quartz are completely consumed during melting. Quartz is consumed between 925 and 950° C. Plagioclase is consumed between 975 and 1025° C and extrapolation of the phase abundance curve suggests that plagioclase-out occurs at approximately 1000° C (Fig. 2b). Amphibole is present in all of the samples, but its abundance decreases monotonically with increasing temperature. Extrapolation of the amphibole abundance curve suggests that amphibole-out is at approximately 1060° C (Fig. 2b).

The 2.0 GPa results are shown in Fig. 2c. Melt, clinopyroxene and product garnet are present in all runs, but they occur only in trace amounts at 800° C. There are significant quantities of melt, clinopyroxene and garnet present at 900° C. Extrapolation of abundance curves of the product phases (melt, clinopyroxene and garnet) suggests that the effective solidus is between 800 and 850° C at 2.0 GPa and we arbitrarily locate it at 825° C. Both plagioclase and quartz are completely consumed between 800 and 900° C and amphibole is consumed by 950° C. Based on unconstrained extrapolations of their abundance curves, we suggest that plagioclase and quartz are consumed between 850 and 900° C.

Fig. 2a, b Plots of phase proportions versus temperature for: **a** 1.5 GPa runs (t = 24 h) **b** 1.5 GPa runs (t = 96–216 h) and **c** 2.0 GPa experiments. *Dotted lines* are extrapolations

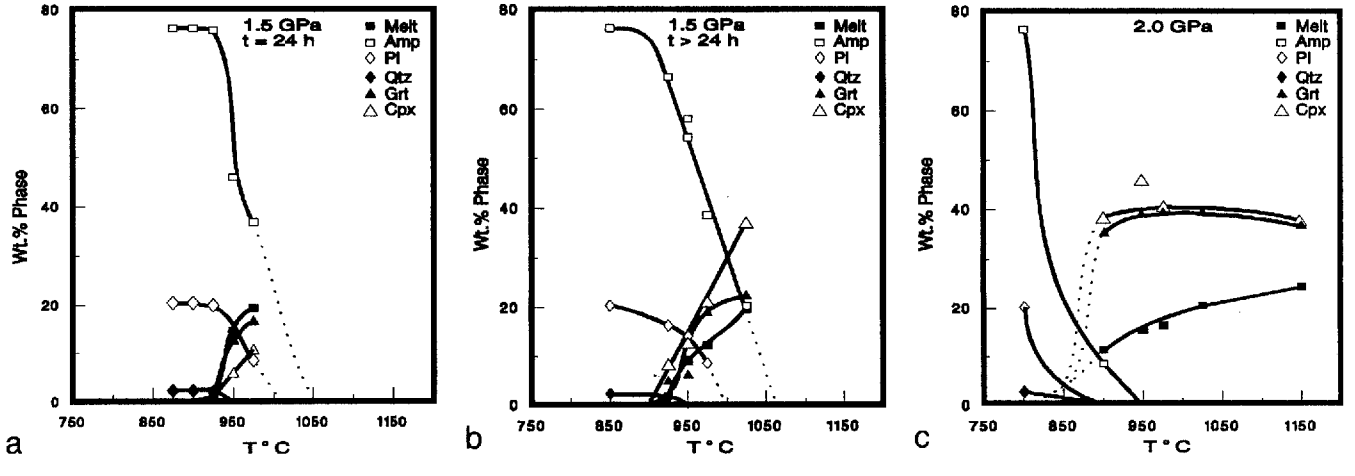

Table 3 Average mineral compositions from experiments. Numbers in brackets are the one sigma standard deviations of the averages expressed in units of the least significant figure reported

Run	Phase	n	SiO_2	TiO_2	Al_2O_3	MgO	CaO	MnO	FeO*	Na_2O	K_2O	Total
B7	Grt	5	39.06(55)	0.69(25)	21.18(42)	5.03(25)	11.04(56)	1.12(20)	22.41(38)	n.d.	n.d.	100.53
	Amp	3	43.60(25)	1.50(2)	12.17(45)	10.63(25)	11.74(10)	0.25(2)	16.29(41)	1.60(5)	0.75(1)	98.53
	Ampr	6	43.82(78)	1.42(6)	12.55(80)	10.78(27)	11.49(20)	0.22(2)	15.29(65)	1.65(19)	0.80(7)	98.02
B1	Grt	4	38.23(35)	0.98(10)	20.78(24)	5.32(42)	10.37(65)	1.00(15)	23.3(10)	n.d.	n.d.	100.08
	Amp	6	42.94(64)	1.48(8)	12.35(35)	10.34(55)	11.58(34)	0.26(11)	16.03(68)	1.61(10)	0.79(9)	97.38
	Pl	4	53.81(38)	n.d.	28.21(15)	n.d.	11.02(2)	n.d.	0.50(4)	5.13(23)	0.25(3)	98.92
B2	Grt	5	38.62(43)	1.18(21)	20.59(30)	6.56(25)	8.35(52)	0.86(14)	23.44(48)	n.d.	n.d.	99.70
	Amp	10	42.58(47)	1.56(16)	12.15(64)	10.56(22)	11.44(46)	0.21(6)	12.15(64)	1.58(12)	0.83(5)	96.45
	Pl	3	54.54(31)	n.d.	27.58(14)	n.d.	10.80(31)	n.d.	0.59(3)	5.26(12)	0.16(3)	98.34
B3	Grt	6	38.55(48)	1.44(10)	20.30(72)	6.96(12)	8.77(68)	0.72(7)	22.95(60)	n.d.	n.d.	99.69
	Amp	7	42.43(40)	1.42(11)	12.14(37)	10.54(32)	11.26(39)	0.26(9)	15.95(67)	1.62(7)	0.78(3)	96.40
	Pl	3	54.94(56)	n.d.	27.85(23)	n.d.	10.95(25)	n.d.	0.68(15)	5.21(18)	0.25(4)	99.88
B18	Grt	5	39.27(44)	1.19(27)	20.35(49)	7.42(70)	9.49(64)	0.65(26)	21.51(30)	n.d.	n.d.	100.06
	Cpx	6	50.52(75)	0.86(20)	7.65(77)	11.23(27)	18.23(44)	n.d.	10.41(61)	1.42(25)	n.d.	100.32
	Amp	5	43.15(22)	1.48(10)	12.24(54)	10.92(13)	11.68(27)	0.24(3)	15.91(24)	1.57(11)	0.82(3)	98.01
	Ampr	7	43.73(92)	1.80(40)	12.35(64)	11.21(41)	11.52(58)	0.21(4)	14.4(14)	2.08(34)	0.82(8)	98.12
B4	Grt	6	39.01(33)	1.42(30)	21.15(11)	8.41(33)	7.52(40)	0.41(5)	22.24(24)	n.d.	n.d.	100.26
	Cpx	6	50.65(53)	0.74(17)	5.9(13)	12.5(12)	15.9(19)	n.d.	13.5(18)	0.90(23)	n.d.	100.09
	Amp	5	42.89(56)	1.43(8)	12.29(32)	10.60(27)	11.58(14)	0.26(6)	15.51(36)	1.61(7)	0.81(4)	96.98
	Pl	3	54.77(29)	n.d.	27.93(32)	n.d.	10.98(16)	n.d.	0.43(18)	5.18(24)	0.25(5)	99.40
M4	Grt	4	39.41(44)	1.18(40)	20.75(44)	7.47(62)	9.20(39)	0.52(6)	21.36(65)	n.d.	n.d.	99.89
	Cpx	12	51.55(49)	1.11(6)	8.1(11)	10.53(36)	18.71(42)	n.d.	7.53(41)	2.25(36)	n.d.	99.77
	Amp	4	42.50(36)	1.50(7)	13.05(23)	11.70(43)	11.70(32)	n.d.	15.65(38)	1.55(18)	0.81(11)	96.15
	Ampr	4	42.48(56)	1.90(45)	12.97(45)	11.40(68)	11.40(70)	n.d.	12.8(12)	2.57(25)	0.77(6)	96.54
M5	Grt	4	39.16(28)	1.24(18)	20.80(12)	8.75(13)	8.51(25)	0.62(7)	20.87(28)	n.d.	n.d.	99.95
	Cpx	7	50.7(10)	0.89(18)	8.87(95)	11.92(64)	16.16(31)	n.d.	8.96(66)	2.75(27)	n.d.	100.25
	Amp	3	42.86(29)	1.55(6)	12.31(61)	10.77(18)	11.60(8)	0.28(8)	15.70(50)	1.66(20)	0.82(8)	98.38
	Ampr	9	42.87(29)	1.76(24)	13.12(77)	11.92(64)	11.10(31)	n.d.	12.9(11)	2.75(27)	0.81(5)	97.92
B5	Grt	5	38.64(46)	1.93(10)	20.95(32)	8.73(13)	7.24(32)	0.42(10)	22.18(17)	n.d.	n.d.	100.18
	Cpx	5	49.82(75)	0.82(19)	6.7(15)	12.23(80)	18.13(9)	0.28(5)	12.3(15)	1.34(20)	n.d.	101.37
	Amp	4	42.51(40)	1.50(17)	12.11(13)	10.67(30)	11.51(20)	0.24(6)	15.87(12)	1.64(4)	0.83(3)	96.88
	Pl	3	54.60(12)	n.d.	28.60(16)	n.d.	10.60(15)	n.d.	0.45(23)	5.50(16)	0.20(5)	99.95
M2	Grt	6	39.71(45)	1.07(16)	21.70(27)	8.73(28)	8.89(21)	0.44(11)	20.07(38)	n.d.	n.d.	100.61
	Cpx	7	50.39(50)	1.02(9)	8.20(71)	10.98(35)	18.44(89)	n.d.	9.3(15)	1.47(26)	n.d.	99.76
	Amp	5	42.26(61)	1.67(14)	12.21(23)	11.17(42)	11.40(34)	n.d.	15.22(48)	1.71(18)	1.21(12)	96.95
	Ampr	4	41.14(54)	3.57(42)	15.35(61)	11.58(51)	10.22(24)	n.d.	11.72(49)	3.01(20)	1.20(14)	97.79
	Pl	5	54.60(36)	n.d.	28.50(45)	n.d.	10.55(15)	n.d.	0.58(2)	6.00(1)	0.20(5)	100.43
B14	Grt	12	38.90(58)	1.37(34)	21.15(38)	8.81(24)	8.99(21)	0.42(14)	20.25(66)	n.d.	n.d.	100.09
	Cpx	8	48.40(96)	1.18(20)	9.1(14)	11.05(50)	17.5(17)	0.24(9)	10.7(21)	1.40(25)	n.d.	99.58
	Amp	5	42.68(98)	1.93(43)	12.91(41)	11.32(34)	11.11(21)	n.d.	13.9(12)	2.83(15)	0.82(6)	97.59
	Ampr	7	40.79(17)	4.03(47)	14.35(21)	10.86(26)	10.02(32)	n.d.	13.6(15)	3.10(13)	0.93(2)	97.28
B17	Grt	8	39.34(23)	0.87(14)	21.84(33)	9.23(18)	8.43(41)	0.45(7)	19.85(22)	n.d.	n.d.	100.01
	Cpx	5	48.45(24)	1.16(22)	9.96(41)	9.90(43)	18.00(34)	n.d.	9.83(25)	1.93(5)	n.d.	99.38
	Amp	4	43.24(35)	1.51(24)	12.50(43)	11.18(27)	11.65(26)	0.34(12)	15.60(75)	1.82(25)	0.70(7)	98.54
	Ampr	5	40.88(50)	3.16(42)	14.87(36)	11.15(15)	10.06(18)	n.d.	13.96(22)	3.06(12)	0.80(8)	98.99
B8	Grt	10	39.04(36)	1.24(17)	21.10(47)	7.78(78)	9.7(12)	0.38(8)	20.58(35)	n.d.	n.d.	99.92
	Cpx	14	52.2(11)	0.75(17)	9.8(12)	9.73(61)	16.02(67)	n.d.	7.30(62)	3.90(70)	n.d.	99.71
	Bt	2	38.82(15)	4.75(30)	16.00(16)	13.59(24)	0.60(32)	n.d.	11.30(17)	0.55(3)	8.72(24)	94.33
	Kfsp	4	66.13(45)	0.12(6)	19.37(38)	n.d.	0.33(24)	n.d.	0.31(12)	5.5(13)	9.0(23)	100.73
B16	Grt	5	39.01(11)	1.43(48)	21.15(60)	8.61(17)	8.93(35)	0.39(10)	20.15(26)	n.d.	n.d.	99.70
	Cpx	9	51.92(78)	1.05(6)	9.8(13)	10.14(46)	16.43(48)	n.d.	7.67(55)	3.45(31)	n.d.	100.46
M6	Grt	9	39.33(75)	1.38(28)	21.28(41)	9.00(67)	9.48(32)	0.40(8)	18.98(40)	n.d.	n.d.	99.99
	Cpx	16	51.3(10)	0.94(10)	9.06(95)	11.06(55)	16.67(84)	n.d.	7.9(13)	3.01(47)	n.d.	99.99
B9	Grt	10	39.23(44)	1.31(42)	20.66(66)	8.88(67)	9.38(65)	0.42(15)	19.94(34)	n.d.	n.d.	99.97
	Cpx	12	50.51(26)	1.34(8)	8.60(38)	10.57(20)	17.57(48)	n.d.	8.57(34)	2.80(17)	n.d.	99.96
D28	Grt	16	39.19(46)	0.87(39)	21.44(78)	9.82(44)	8.77(84)	0.44(8)	18.51(69)	n.n.	n.d.	99.14
	Cpx	11	49.42(60)	0.90(14)	9.2(12)	11.06(50)	17.60(41)	n.d.	8.91(24)	1.93(17)	n.d.	99.02

(*Grt* garnet, *Cpx* clinopyroxene, *Amp* amphibole, *Ampr* amphibole rim, *Pl* plagioclase, *Bt* bitotite, *Kfsp* K-feldspar, *nd* not detected, * total iron as FeO)

Garnet

The garnets are relatively homogeneous in composition in a given experimental charge (Table 3). The original garnets from the starting material are preserved in the cores of newly crystallized garnets. Product garnets have higher TiO_2 and MgO contents and lower MnO and CaO contents than the original garnet (Tables 1 and 3). Figure 3 shows the grossular, pyrope and almandine + spessartine components of the product garnets relative to original garnet. At both pressures, the pyrope content of garnet increases with increasing temperature along a vector approximately perpendicular to the grossular - almandine + spessartine join.

Garnet-melt Fe-Mg exchange K_Ds, calculated from the average garnet and melt analyses for each run (long runs only), assuming total iron was FeO in both phases, decrease abruptly with increasing temperature from approximately 0.8 to approximately 0.6 between 950 and 975° C at both 1.5 and 2.0 GPa. Garnet-melt K_Ds are more varied in the lower temperature runs ($T \leq 950$° C) than in the higher temperature runs ($T \geq 975$° C) due to greater scatter in garnet compositions and low MgO contents (with associated large uncertainties) in the melts. This result strongly suggests that garnet/melt Fe-Mg exchange equilibrium was not achieved in runs at temperatures below 975° C.

Omphacitic clinopyroxene

At temperatures below 900° C clinopyroxene compositions are quite variable, apparently in response to localized melting and incomplete equilibration. Typical compositions of clinopyroxenes in 925° C and higher temperature runs are listed in Table 3. Figure 4 shows variations in the quadrilateral components of the pyroxenes. In general, the clinopyroxenes from a single run plot approximately parallel to En isopleths over a considerable range of Wo and Fs contents. The 1.5 GPa data from all runs plot in a narrow band extending from approximately $Wo_{35}En_{40}Fs_{25}$ to $Wo_{20}En_{35}Fs_{45}$ and there is almost complete overlap of the data from the various runs (Fig. 4a). The 2.0 GPa data plot in a broader band (i.e., from approximately En_{35} to En_{42}) extending from approximately $Wo_{35}En_{40}Fs_{25}$ to $Wo_{22}En_{38}Fs_{40}$ (Fig. 4b). There is some suggestion that the En content of the pyroxenes decreases with increasing temperature, but the variation is not systematic. Variations of the CaTs and jadeite components are plotted versus temperature in Fig. 5. The CaTs component increases with temperature at 1.5 GPa, but, with the exception of the 1150° C point, is essentially constant at 2.0 GPa (Fig. 5a). Jadeite decreases with increasing temperature at both pressures (Fig. 5b). With increasing pressure the CaTs component decreases while the jadeite component increases.

Calculated Fe-Mg exchange K_Ds for clinopyroxene-melt pairs (assuming total iron is FeO in both phases) have a wide range of values in the lower temperature (< 950° C) runs, due to the compositional heterogeneity of the clinopyroxenes and low MgO contents of the

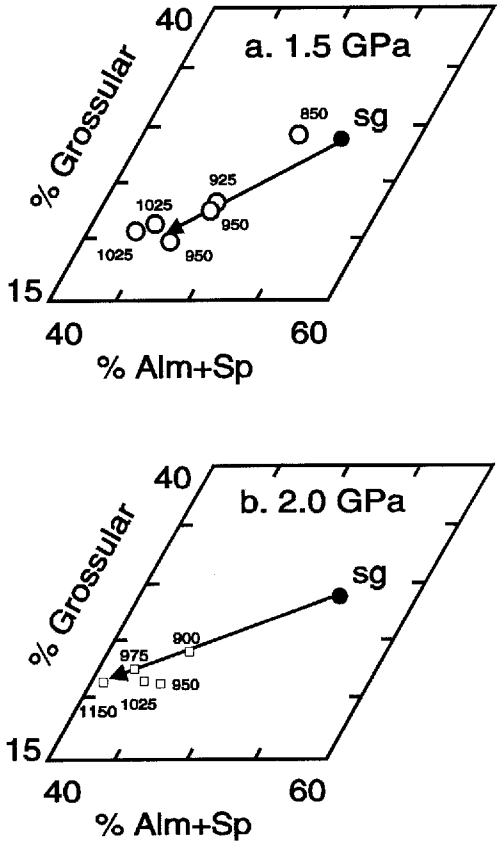

Fig. 3a, b Compositions of garnets produced at 1.5 GPa **(a)** and 2.0 GPa **(b)** projected into a molar grossular-pyrope-almandine + spessartine triangular plot

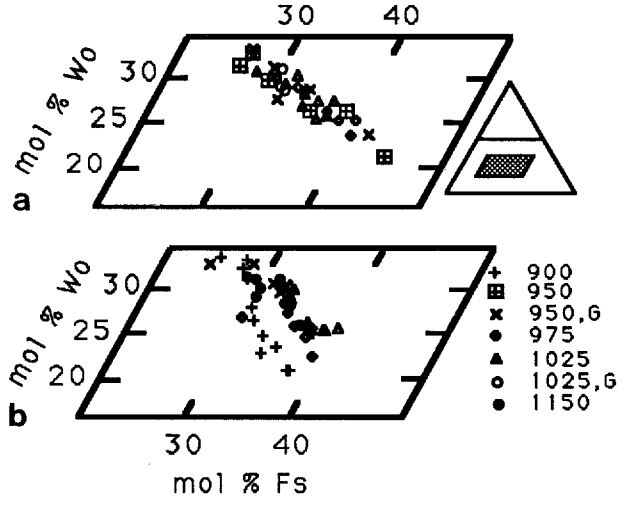

Fig. 4a, b Compositions of omphacitic clinopyroxenes projected into the pyroxene quadrilateral using the Lindsley (1983) projection scheme. **a** 1.5 GPa results, **b** 2.0 GPa results

melts. At both pressures, average K_D values range from 0.19 to 0.25, which is within the expected range of equilibrium values for high pressure clinopyroxenes (e.g., Grove and Bence 1977; Nielsen and Drake 1979).

Amphibole

The average compositions of amphiboles are given in Table 3. Relative to the original amphibole, increases in Na_2O, TiO_2 and Al_2O_3 contents in the newly developed amphiboles and in rims on pre-existing amphiboles are accompanied by decreases in SiO_2, FeO* and CaO. No systematic relationships were found between amphibole composition and temperature. However, with increasing temperature, core and rim compositions of amphiboles became more similar (Table 3). Amphibole-rim/melt Fe-Mg exchange K_Ds also have a limited range of values (0.55 to 0.62) at 1.5 GPa.

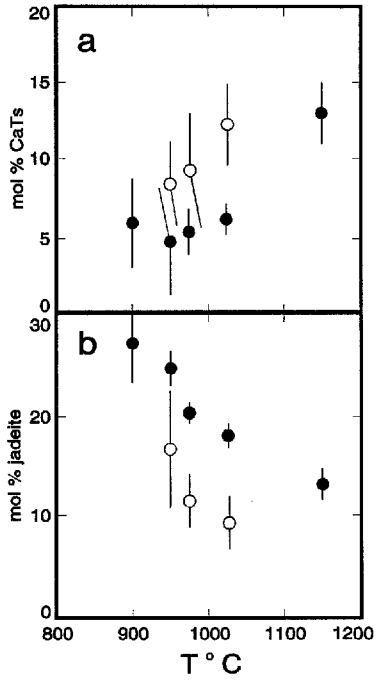

Fig. 5a, b Variations in CaTs **(a)** and jadeite **(b)** components of clinopyroxenes (Lindsley 1983 projection scheme) as functions of temperature. *Open circles* represent 1.5 GPa results and *filled circles* show 2.0 GPa results

Melts

The compositions of melts in the runs range from andesitic to rhyolitic (anhydrous basis) depending upon temperature and pressure (Table 4). Melts are produced locally and are not homogeneous in composition in runs below 950° C (24 h runs) and 925° C (longer runs) at 1.5 GPa and these melt compositions are not reported in Table 4.

The major element compositions of the melts produced in the 1.5 GPa (longer runs) and 2.0 GPa runs are plotted as a function of temperature in Fig. 6. At both pressures, the SiO_2 and K_2O contents of the melts decrease with increasing temperature. At 1.5 GPa the average values of TiO_2, Al_2O_3, FeO*, MgO, CaO and Na_2O in 1.5 GPa melts increase slightly with increasing temperature (Fig. 6a). On the other hand, large systematic increases in all components, except SiO_2 and K_2O which decrease, are clearly observed in the 2.0 GPa runs (Fig. 6b). In general, compared to the 2.0 GPa runs (average analysis basis), the 1.5 GPa melts are less aluminous, sodic and potassic. The most alkali-rich melts were produced in the lowest temperature runs. While, Mg-numbers of melts in a given experimental charge vary from 0.20 to 0.42, average Mg-numbers are fairly constant around 0.30. The melts from the gold

Table 4 Average melt compositions in the experiments. The analyses have been renormalized to 100% to facilitate comparison. Original totals are given. Numbers in brackets are the one sigma standard deviations of the averages expressed in units of the least significant figure reported. (*total iron expressed as FeO, *nd.* not detected)

Run	n	SiO_2	TiO_2	Al_2O_3	MgO	CaO	MnO	FeO*	Na_2O	K_2O	Total
						1.5 GPa Experiments					
B18	3	69.49(92)	0.26(8)	16.71(36)	0.35(17)	1.52(42)	n.d.	1.35(10)	4.48(80)	5.85(65)	93.85
B4	6	70.09(77)	0.54(5)	16.10(28)	0.69(10)	2.52(11)	n.d.	2.38(11)	4.64(15)	3.05(6)	93.31
M4	7	67.56(80)	0.63(5)	17.64(17)	0.74(19)	2.35(33)	n.d.	2.37(11)	5.63(77)	3.09(8)	91.68
M5	5	66.36(95)	0.61(6)	18.01(30)	0.85(16)	3.36(31)	n.d.	3.13(30)	5.18(52)	2.51(11)	91.77
B5	5	68.10(65)	0.80(7)	17.08(11)	0.92(12)	2.87(11)	n.d.	2.98(10)	4.65(21)	2.84(2)	93.06
M2	7	65.29(29)	0.76(5)	18.53(20)	0.72(6)	2.63(6)	n.d.	2.85(12)	6.49(20)	2.73(3)	92.17
B14	8	61.67(47)	1.05(5)	19.02(27)	1.16(12)	3.07(14)	n.d.	4.75(10)	6.54(10)	2.84(3)	93.30
B17	5	62.81(66)	1.06(7)	18.36(19)	1.29(25)	3.52(33)	n.d.	4.81(20)	5.53(33)	2.61(7)	93.09
						2.0 GPa Experiments					
B8	8	71.16(49)	0.30(4)	15.95(17)	0.36(16)	1.04(38)	n.d.	1.20(18)	4.74(23)	5.24(18)	92.96
B16	6	67.66(78)	0.61(5)	17.45(24)	0.62(23)	1.61(47)	n.d.	1.89(15)	4.89(36)	5.29(18)	92.08
M6	6	66.18(51)	0.78(4)	17.81(21)	0.68(12)	1.88(10)	n.d.	2.48(14)	5.70(20)	4.50(6)	91.42
B9	6	62.00(93)	1.46(12)	18.34(22)	1.18(21)	2.81(27)	n.d.	4.39(46)	6.08(22)	3.74(9)	90.89
D28	7	56.40(90)	2.29(9)	17.61(48)	2.14(48)	5.61(58)	n.d.	7.55(66)	5.91(87)	2.49(19)	92.27

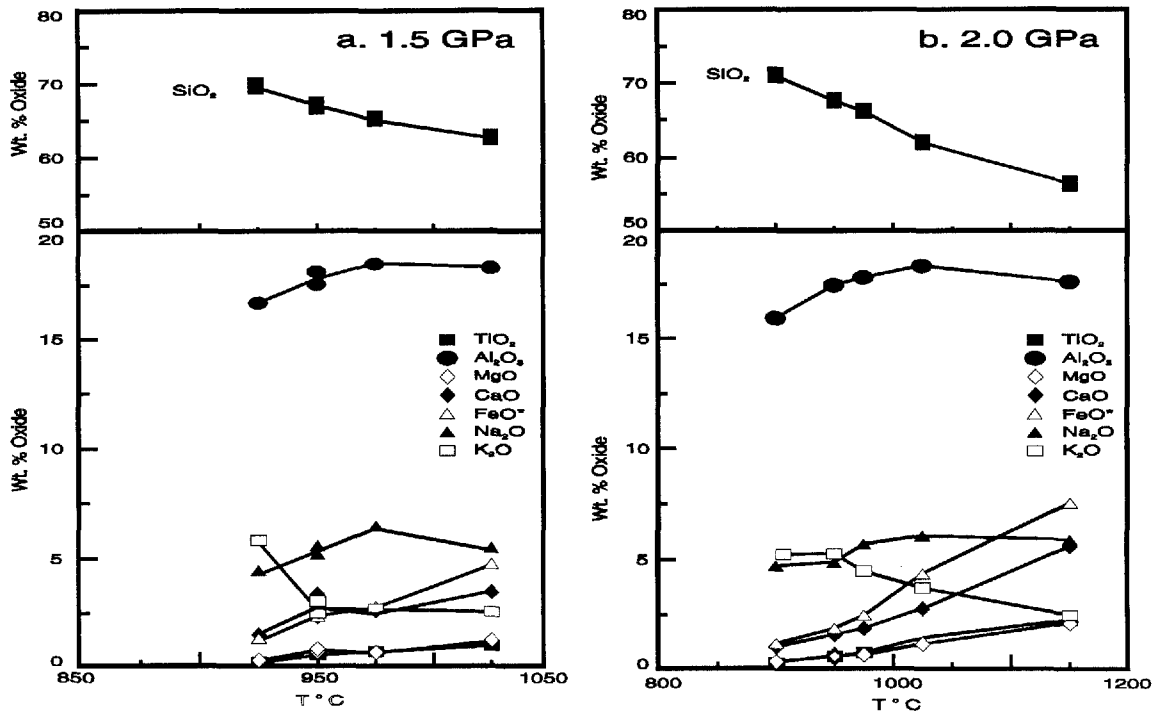

Fig. 6a, b Variation in melt composition as a function of temperature in 1.5 GPa **(a)** and 2.0 GPa **(b)** runs. Compositional uncertainities (Table 4) are not shown for reasons of clarity

capsule runs are slightly CaO enriched relative to Pt-C capsule runs, but are otherwise similar.

Dehydration melting reactions

24 hour experiments

Preliminary experiments of 24 h duration were conducted at 1.5 GPa, using relatively coarse grained (− 60/ + 120 mesh) starting material to determine approximately the dehydration melting relationships. At temperatures up to 925° C the melting is local, melt makes up less than 1 vol.% of the samples, and the reaction products are heterogeneous in composition. During this first melting stage, four melting relations are identified based on textural and melt composition criteria:

$$\text{amp} + \text{qtz} \rightarrow \text{melt I} + \text{cpx I} \quad (1)$$

$$\text{amp} + \text{pl} + \text{qtz} \rightarrow \text{melt II} + \text{cpx II} + \text{grt} \quad (2)$$

$$\text{amp} + \text{pl} \rightarrow \text{melt III} + \text{cpx III} + \text{grt} \quad (3)$$

$$\text{amp} \rightarrow \text{melt IV} + \text{cpx IV} \quad (4)$$

Clinopyroxenes of different composition are produced by these reactions and the dehydration of amphiboles (amp → cpx V + vapor). Between 925 and 950° C, quartz reacts out and a significant increase in melting occurs. Similar reaction relations have also been identified by Rapp et al. (1991) and Wolf (1992).

Longer (> 24 hours) experiments at 1.5 and 2.0 GPa

The phase proportions in the samples (Table 2) are plotted as a function of melt proportion in Fig. 7. The slopes of the phase abundance curves indicate the stoichiometry of the melting reaction, where negative and positive slopes indicate reactant and product phases, respectively. Figure 7a shows that the 1.5 GPa results are consistent with two melting reactions. At lower temperatures the weight proportion melting reaction is approximately:

$$0.24\ \text{qtz} + 0.6\ \text{pl} + 2.16\ \text{amp} \rightarrow 1.22\ \text{cpx} + 0.86\ \text{grt} + 1.0\ \text{melt} \quad (5)$$

The melting proportions of the original amphibolite phases (qtz : pl : amp) are 8 : 20 : 72, compared to abundance proportions of 2.3 : 20.5 : 76.3 for the starting amphibolite. The non-modal nature of the melting reaction is consistent with the order of disappearance of the phases (Table 2). When quartz reacts out of the assemblage (between 925 and 950° C), the melting reaction changes to:

$$3.6\ \text{amp} + 1.0\ \text{pl} \rightarrow 2.2\ \text{cpx} + 1.5\ \text{grt} + 1.0\ \text{melt} \quad (6)$$

The melting proportions of plagioclase and amphibole in reaction 6(24 : 76; pl : amp) are approximately modal, based on the plagioclase: amphibole ratio at quartz-out calculated from the initial mode using reaction 5 (21 : 79), but the melting reaction is consistent with

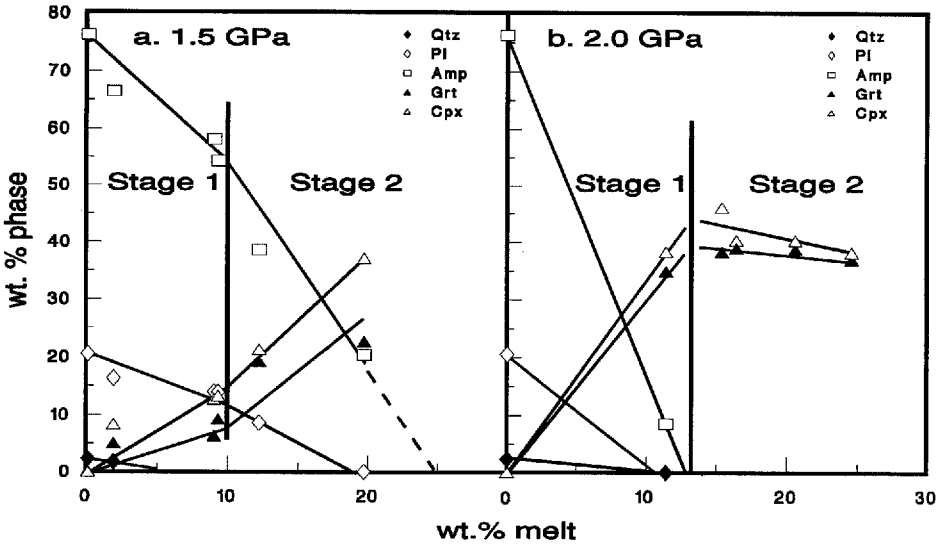

Fig. 7a, b Phase proportions from the experiments plotted against melt proportion. Reactions and reaction coefficients were determined from the slopes of the phase abundance curves. **a** The 1.5 GPa data are consistent with two stages of melting reactions (reactions 5 and 6). **b** The 2.0 GPa results are also consistent with two stages of melting (reactions 7 and 8)

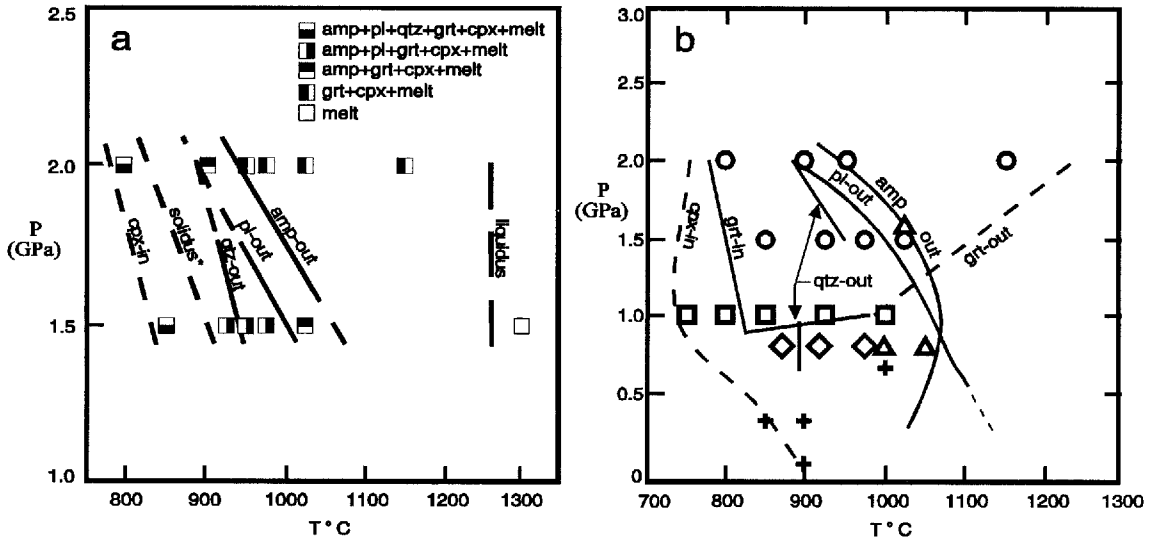

Fig. 8a, b *P-T* phase diagram of the amphibolite studied and a composite phase diagram for amphibolite dehydration melting. **a** Phase diagram of the amphibolite investigated in this study. *Solid lines* show well constrained boundaries and *dashed lines* are interpreted boundaries. Solidus* is the inferred effective solidus (i.e. where melting exceeds > 1%). **b** Composite phase diagram for dehydration melting of basaltic composition amphibolites (*circles*, this study; *squares*, Wolf 1992; *crosses*, Beard and Lofgren 1991; *triangles*, Rapp et al. 1991; *diamonds*, Rushmer 1991)

plagioclase-out occurring before amphibole out as observed.

The 2.0 GPa phase abundance versus melt fraction curves (Fig. 8b) are also consistent with two melting reactions. The low temperature reaction is:

$$4.95\ \text{amp} + 1.80\ \text{pl} + 0.20\ \text{qtz} \rightarrow 1.00\ \text{melt} + 3.00\ \text{cp0x} + 2.49\ \text{grt} \quad (7)$$

The melting proportions from reaction 7 (3:26:71; qtz:pl:amp) are consistent with quartz and plagioclase reacting out before amphibole. The persistence of amphibole after quartz- and plagioclase-out indicates that there must be either a period of amphibole melting or a period of amphibole + clinopyroxene + garnet melting, that occurs until amphibole reacts out of the system. Unfortunately, the data are not sufficient to define that reaction. After amphibole-out, the melting reaction is approximately:

$$0.86\ \text{cpx} + 0.14\ \text{grt} \rightarrow 1.00\ \text{melt} \quad (8)$$

Reaction 8 is consistent with clinopyroxene reacting out of the system at approximately 60% melting to leave a garnet restite.

Ideally, the melting reactions should have equal amounts of products and reactants. Reactions 5, 6 and 7 are not balanced (masses of products, P, and reactants, R, are P = 3.08, R = 3.00, reaction 5; P = 4.7, R = 4.6, reaction 6; R = 6.95, P = 6.49, reaction 7). The

reactions were determined from changes in phase proportions over a range of tempertures, which does not constrain the reactions to balance. The discrepancies may be due to changes in reaction stoichiometry with temperature that are not accounted for and/or errors in the determinations of the phase abundances. Given those factors, the approach to balance is thought to be acceptable.

Phase relations

Figure 8a shows the phase relationships of the amphibolite as a function of temperature and pressure. The locations of the phase boundaries are drawn based on a combination of experimental brackets, extrapolations of phase abundance curves versus temperature (i.e., Fig. 2) and the derived melting reactions. We interpret clinopyroxene-in to be coincident with the onset of melting. Our lowest temperature runs at both pressures contained trace amounts of clinopyroxene and melt. Those runs provide a high temperature limit for the location of the clinopyroxene-in curve, but the curve is not bracketed on the low temperature side. Thus, the clinopyroxene-in curve is drawn on the low temperature side of our lowest temperature runs. While melt is present in all runs, the melts in the low temperature runs are heterogeneous in composition and apparently not interconnected. The "solidus" curve in Fig. 8a is drawn to coincide with our interpretation of the temperatures at which the melts become interconnected (at approximately 1–2 wt% melting). Thus that curve is an effective solidus. As noted above, the true solidus lies at temperatures below those investigated here. The quartz-out curve is located between 925 and 950° C at 1.5 GPa and 850 and 900° C at 2.0 GPa. The plagioclase-out curve falls between 975 and 1025° C at 1.5 GPa and 800 and 900° C at 2.0 GPa. The amphibole-out curve was not bracketed at 1.5 GPa and lies between 900 and 950° C at 2.0 GPa. The locations of those curves are drawn based on extrapolations of phase abundance versus temperature curves (Fig. 2). The liquidus is at less than 1300° C at 1.5 GPa and greater than 1150° C at 2.0 GPa, but is otherwise unconstrained.

The results of this study were combined with data from the literature to construct a composite phase diagram for basaltic amphibolite dehydration melting (Fig. 8b). Only results for compositions similar to that used in this study were used to construct the diagram. The data used were: composition 466 (Beard and Lofgren 1991), composition ABA (Rushmer 1991), composition WR-40 (Rapp et al. 1991) and all results (Wolf 1992). The amphibolite compositions, used to construct the composite phase diagram, cluster around the plane of silica saturation in a molar CMS ternary, and are close to N-MORB (Hofmann 1988). The compositions used by Wolf (1992) and in this study are silica undersaturated, while those of Beard and Lofgren (1991), Rushmer (1991) and Rapp et al. (1991) are silica saturated as is N-MORB.

Figure 8b shows the composite phase diagram. For simplicity, only the experimental data points which are used to bracket the phase boundaries are shown. The solidus is not shown. Instead, we show the approximate location of clinopyroxene-in, which we have interpreted to be coincident with the solidus. The location of that curve is constrained by Beard and Lofgren's (1991) 850/900° C bracket at 0.3 GPa, Wolf's (1992) identification of clinopyroxene at 750° C and 1.0 GPa and our identification of clinopyroxene at 800° C and 2.0 GPa. Rushmer (1991) reported the solidus between 875 and 925° C at 0.8 GPa, but that point was not used because of the lower temperature result reported by Wolf (1992) at 0.8 GPa.

Garnet appears only at pressures above 1.0 GPa (Fig. 8b). Only Wolf (1992) bracketed the garnet-in curve between 800 and 850° C at 1.0 GPa. Their result, extrapolated to higher pressure assuming a negative dP/dT slope, is consistent with our observation of product garnet at 800° C and 2.0 GPa. The garnet in curve is drawn on the low temperature side of our 800° C point at 2.0 GPa to a point between 800 and 850° C at 1.0 GPa and is then isobaric to 1000° C, where Wolf (1992) observed that garnet reacted out. A schematic garnet-out curve is drawn with a positive dP/dT slope extending from 1000° C and 1.0 GPa to higher pressures and temperatures, but the location of that curve is unconstrained.

Only two studies had quartz in the starting material (Rushmer 1991; this study). Rushmer bracketed quartz-out between 880 and 920° C at 0.8 GPa. We interpret quartz-out to be at approximately 950° C at 1.5 GPa and just below 900° C at 2 GPa. Our results are not consistent with Rushmer's results assuming a constant dP/Dt slope for the quartz-out curve. Therefore, Fig. 8b shows both results for quartz-out. The plagioclase-out curve is drawn based on our results at 1.5 and 2 GPa and the stability limit determined by Rapp et al. (1991) at 0.8 GPa. The thermal stability of plagioclase in amphibolite dehydration melting appears to be proportional to the anorthite content of the plagioclase (i.e., more anorthitic plagioclase persists to higher temperature than comparatively albitic plagioclase) and is also related to the water content of the partial melt (Rapp et al. 1991). Thus, the location of the plagioclase-out curve in Fig. 8b is only an approximation and will vary as a function of the Ca/Na ratio and the water content of the amphibolite being melted.

The amphibole-out curve shown in Fig. 8b is based on our results at 1.5 and 2 GPa and the results of Rapp et al. (1991) at 0.8 and 1.6 GPa. The thermal stability of amphiboles depends on their major element and volatile compositions as well as pressure. Amphiboles with higher Mg-numbers are stable to higher temperatures than more iron-rich amphiboles and K-rich

amphiboles have higher pressure stability limits than more sodic amphiboles (e.g. Gilbert et al. 1982). Structural F and Cl also stabilize amphiboles to higher temperatures relative to pure hydroxyl amphiboles (e.g., Gilbert et al. 1982). Given those considerations, the location of the amphibole-out curve in Fig. 8b is only approximate.

Melt compositions

The melt compositions determined this study are compared with the results of other amphibolite dehydration melting studies (Rapp et al. 1991; Rushmer 1991; Wolf 1992) in Fig. 9. Normative albite, anorthite and orthoclase were calculated from each analysis on an anhydrous basis assuming total iron as FeO. The compositions of the melts produced in this study shift from granitic to trondhjemitic with increasing temperature at both pressures studied. Only the highest temperature runs produced tonalitic melts. The compositional trend shows that with increasing temperature, at both pressures, amphibolite melting produces tonalitic melts. The only melts that plot in the granite field are from runs that included quartz in the restite. It appears that the presence of quartz buffers the silica content of the melt at relatively high values. Once quartz reacts out of the system, the melt compositions shift to lower silica contents and move out of the granite field in Fig. 9 into the trondhjemite and tonalite fields with increasing melting.

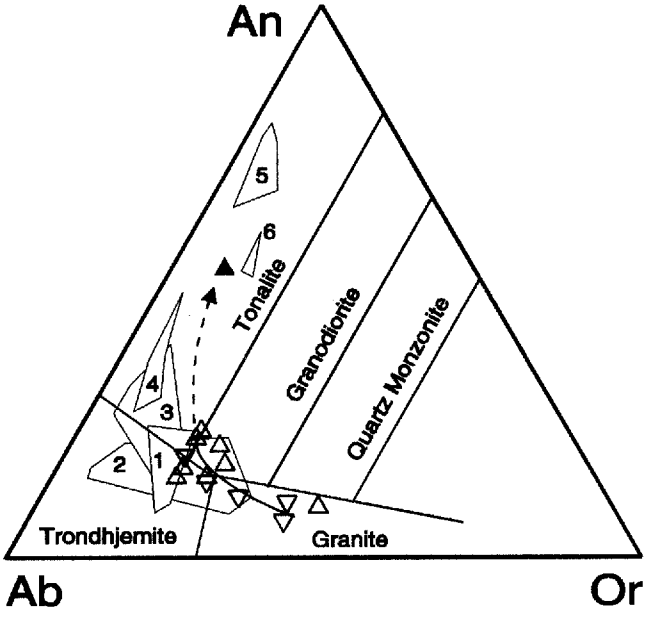

Fig. 9 Normative albite (Ab)- anorthite (An)- orthoclase (Or) plot showing melt compositions from amphibolite dehydration studies (anhydrous basis). The *filled triangle* shows our starting composition. *Apex-up triangles* are our 1.5 GPa results and *apex-down triangles* show the 2.0 GPa melts. *Numbered fields* show melt compositions from Rapp et al. (1991), 1–4; Wolf (1992), 5; and Rushmer (1991), 6. The *arrow* indicates composition changes for our melts with increasing temperature.

Beard and Lofgren (1991), Rapp et al. (1991), Rushmer (1991) and Wolf (1992) found that alumina saturation of water-undersaturated melts depends on temperature and pressure. In this study, the melt compositions in the low melt fraction runs are mildly peraluminous and shift to metaluminous with increasing temperature and pressure. The low degree partial melts (i.e., 2 wt% melt in run B18) may be water saturated, although the water contents of the melts were not determined. However, the amount of dissolved water in the melts decreases with increasing melting and only runs with over 20 wt% melting produced metaluminous melts.

Petrological applications

Adakites

Defant and Drummond (1990) coined the term "adakites" to describe a group of arc magmas that they interpreted to be partial melts of young (< 25 Ma), relatively hot, subducted oceanic crust. Defant and Drummond (1990, 1993) and Drummond and Defant (1990) identified the following criteria as characteristic of adakites: $SiO_2 \geq 56$ wt%, $Al_2O_3 \geq 15$ wt%, Yb ≤ 1.9 ppm, Y ≤ 18 ppm, Sc < 10 ppm, La/Yb > 20, Zr/Sm > 50, positive Sr and Eu anomalies, and Sr generally greater than 400 ppm. Defant and Drummond (1990) also identified thirteen localities where adakites were found (including: the Aleutian arc, the Cascade arc, Mexico and Central America, southern Chile, Kamchatka, and the Philippines). Since 1990, adakites have been described at additional localities in those areas (i.e., Panama, Defant et al. 1991; Mindanao, Sajona et al. 1993; southern Chile, Kay 1993; the Cascade arc, Defant and Drummond 1993, etc.). Defant and Drummond (1990, 1993) rely heavily on the results of experimental studies of high pressure partial melting of hydrous basaltic rocks to support their arguments. However, only Rapp et al. (1991) and this study have investigated the partial melting behavior of natural basaltic composition amphibolites at conditions at which slab melting is thought to occur.

Major element compositions

Figure 10 shows a comparison of the major element compositions of the melts produced in this study (long duration experiments only) and by Rapp et al. (1991) with a representative selection of igneous rocks that have been called adakites. Our results fall within the adakite field for Al_2O_3, FeO and Na_2O. The 1.5 GPa experimental melts have K_2O contents that plot at the

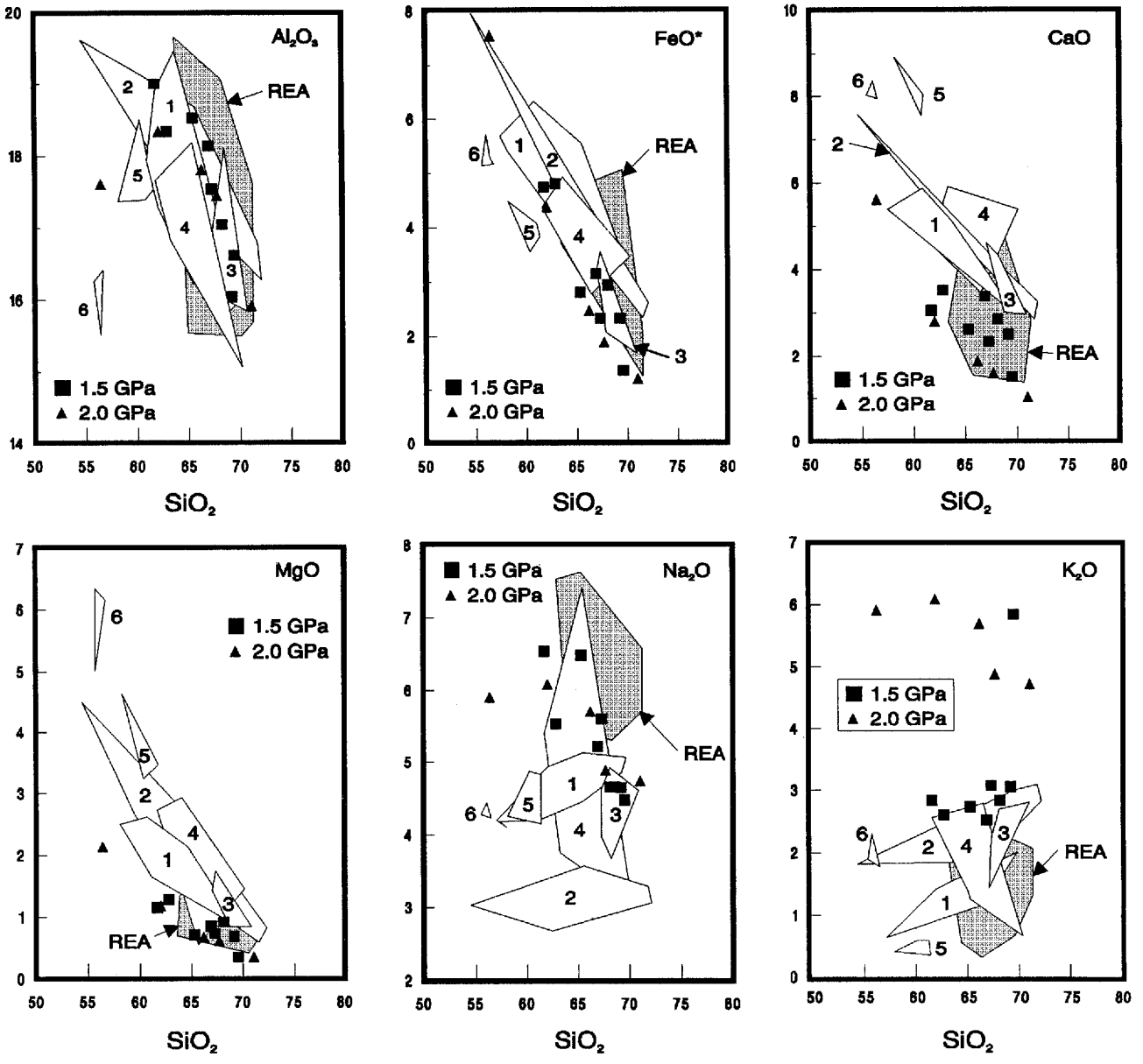

Fig. 10 Comparison of experimentally produced melts with adakites (anhydrous basis). The adakite analyses are from: 1 Mt. St. Helens (Smith and Leeman 1987), 2 Skagway tonalite (Barker et al. 1986), 3 La Yeguada Volcanic Complex, Panama (Defant et al. 1991), 4 Mindanao, Philipines (Sajona et al. 1993), 5 Isla Cook, Patagonia (Puig et al. 1984), 6 Baja California (Rogers et al. (1985). The experimental results of Rapp et al. (1991) are shown as *shaded fields* (REA)

high-K_2O end of the adakite field, but the 2.0 GPa melts have much higher K_2O contents than those reported for adakites. While the experimental data define trends with increasing silica content that are similar to the adakite trends, the CaO and MgO contents of the experimental melts are lower than those of the adakites. The compositions of the melts produced by Rapp et al. (1991) are very similar to those produced in this study and also largely overlap the adakite fields. Again, the experimental melts have lower CaO and MgO contents than the natural samples, but there is more overlap with the adakite fields, particularly for CaO. However, the CaO contents of the Rapp et al. (1991) melts still overlap only the lower half of the range of CaO contents of adakites. The K_2O contents of the Rapp et al. (1991) experimental melts overlap the adakite fields much more than those of the melts produced in this study. In contrast, the Na_2O contents of our melts are more consistent with the natural data than are those of the Rapp et al. (1991) melts. The amphibolites melted by Rapp et al. (1991) had higher Na_2O/K_2O ratios than that used here, which may partly explain the differences between their results and ours. Considering the results of the two experimental studies, it appears that, with the exception of MgO and to a lesser extent CaO, the major element compositions of adakites are consistent

with the compositions of partial melts of amphibolites produced at conditions appropriate to slab melting (i.e., 1.5 to 3.2 GPa and 900 to 1150° C).

Both the present study and that of Rapp et al. (1991) produced melts with low MgO contents relative to adakites. The MgO contents of adakites, at a given silica content, are not as high as those of boninites, but nevertheless are higher than many calc-alkaline volcanics (Rogers and Saunders 1989). The Mg-numbers $[Mg/(Mg + Fe^{2+}) \times 100]$ of adakites are variable and range from 45 to as high as 75. The melts produced by Rapp et al. (1991) have Mg-numbers that average 29 ± 6 and the Mg-numbers of the melts produced in this study average 33 ± 2. Clearly, if adakites are produced by partial melting of subducted oceanic crust, either that crust had a higher Mg-number and CaO content than the amphibolites studied here and by Rapp et al. (1991), or the melts gained MgO and CaO during transport from the melting slab to the surface. Kay (1978) suggested that the high MgO contents of some adakites were produced by interaction of hydrous slab melts with olivine and orthopyroxene in the mantle wedge. Sen and Dunn (1993) and Sen (1994) did experiments in which partial melts of amphibolite reacted with spinel lherzolite. They found that the reactions consumed olivine, clinopyroxene and spinel and precipitated amphibole and Fe-enriched orthopyroxene. The net result of such interactions is to enrich the melts in MgO and, to a lesser extent, CaO. Thus, we suggest that if adakites are the products of slab melting at pressures between 1.5 and 3.2 GPa, then the major element data require that the melts interact with the mantle wedge, during their transport to the surface, and increase their MgO and CaO contents and Mg-numbers. With that caveat, the similarities between the compositions of experimentally produced model slab melts and adakites appear to be sufficient to permit the use of the amphibolite melting relations derived in this study for modelling the trace element characteristics of adakites.

Trace element models

Figure 1 shows the approximate $P - T$ conditions under which slab melting is expected. The approximate locations of the effective dehydration melting solidus, the stability limit of amphibole and the shape of the hot slab geotherm suggest that slab melting begins at approximately 1.5 GPa and reaches its maximum extent at approximately 2 GPa. Thus, the 2.0 GPa amphibolite melting relations derived here (Eqs. 7 and 8) were used to model the trace element compositions of dehydration melts of amphibolite in order to place further constraints on the petrogenesis of adakites. The validity of this modelling study is dependent on having a knowledge the initial mineralogical, modal and trace element composition of the slab and on the use of appropriate mineral/melt trace element partition coefficients. In order to approximate natural systems, N-MORB (Table 5) was used as the initial trace element composition in the models. Batch melting calculations were done for 1, 2, 5, 10, 15, 20 and 30 wt% melting. The starting mode for the calculations (wt%: amp 71.1, pl 26, qtz 2.9) was selected so that quartz and plagioclase would react out simultaneously to simplify the calculations. The mode is similar to the mode of the amphibolite studied (Table 1), thus the derived melting reactions (Eqs. 7 and 8) should be applicable. Quartz is present in the restite until approximately 15 wt% melting. Consequently, melts produced by up to 15 wt% melting will be quartz saturated and are expected to be broadly dacitic in composition. The restite in the 20 and 30 wt% melting models consists of only garnet and clinopyroxene. Thus, the melts would presumably be more andesitic in composition.

The models require trace element mineral/melt partition coefficients for amphibole, plagioclase, quartz, omphacitic clinopyroxene and garnet for andesitic to dacitic melt compositions. Unfortunately, there are no studies that report the determination of an internally consistent set of partition coefficients for all of the minerals coexisting with a single melt. Therefore, a composite set of partition coefficients must be selected. Martin (1987) modelled the partial melting of a tholeiitic basalt to generate a suite of trondhjemites, tonalites and granodiorites. Consequently, the partition coefficients used by Martin (1987) were adopted for amphibole, plagioclase, clinopyroxene and garnet (Table 5). The partition coefficients for quartz were arbitrarily set to zero.

The batch melting models were calculated using the mass balance equation:

$$C_m = C_i/[f_m + \Sigma(f_i{}^*D_i)] \quad (9)$$

where C_m is trace element concentration the partial melt, C_i is trace element composition of the starting

Table 5 Starting composition and partition coefficients used for partial melting models

El	N-MORB[a] (ppm)	Amp[b]	Pl[b]	Qtz	Grt[b]	Cpx[b]
La	3.895	0.2	0.14	0	0.04	0.1
Ce	12.001	0.3	0.10	0	0.08	0.2
Nd	11.179	0.8	0.069	0	0.2	0.4
Sm	3.752	1.1	0.052	0	1.0	0.6
Eu	1.335	1.3	0.79	0	0.98	0.6
Gd	5.077	1.8	0.044	0	3.8	0.7
Dy	6.304	2.0	0.025	0	11	0.7
Er	4.123	1.9	0.019	0	16	0.6
Yb	3.900	1.7	0.012	0	21	0.6
Lu	0.589	1.5	0.009	0	21	0.6
Sr	113.2	0.36	2.0	0	0.013	0.2
Y	35.82	1.9	0.01	0	16	0.03

[a] Hofmann (1988)
[b] Martin (1987)

material (N-MORB, Hofmann 1988); f_m is the fraction of melt in the system, f_i is the fraction of crystalline phase i, and D_i is the partition coefficient of phase i (Table 5). The phase proportions for each degree of melting were calculated by application of reactions 7 (until amphibole, plagioclase and quartz reacted out) and 8. Those melting reactions are non-modal and the batch models are consequently non-modal batch melting models.

The REE concentrations of the model melts are compared to those of adakites in Fig. 11, which shows chondrite normalized (Anders and Grevesse 1989) REE patterns (Fig. 11a) and plots of Sr/Y versus Y (Fig. 11b). The model REE patterns fall within the field defined by the adakites. However, the shapes of the model REE patterns are not all consistent with the Adakite data set. The models for less than 10 wt% melting produced patterns with low $(La/Yb)_N$ ratios (7.0 to 15.4) compared to adakites, which have $(La/Yb)_N$ ratios greater than 20 (Defant and Drummond 1993). The $(La/Yb)_N$ ratios for the higher extents of partial melting increase to 33.8 at 15 wt% melting (where amphibole, plagioclase and quartz are consumed) and then decrease with further melting ($(La/Yb)_N = 19.6$ at 30 wt% melting). As shown in Fig. 11A, the decrease in the ratios is due to a decrease in La abundance without a corresponding decrease in Yb abundance with increasing melting. Thus, only the 10, 15 and 20 wt% melting models generate adakite-like REE abundances and pattern systematics.

Another characteristic feature of adakites is their high Sr/Y ratios (Sr/Y ranges from approximately 20 to as high as 300, Fig. 11b). Figure 11B shows Sr/Y ratios plotted against Y (ppm) for adakites from five locations and the results of the melting models. Only the 15, 20 and 30 wt% melting models produce Sr/Y ratios in the range of those observed for adakites (squares in Fig. 11B), but none of those results fall into the fields defined by the adakite data. While the Sr/Y ratios are acceptable, the Y contents at which those ratios occur are too low. The difference between the models and the natural data indicates either that the Sr partition coefficients used are too large (i.e., Sr is too compatible in the restite), or that the Sr/Y ratio in the adakite source region is substantially higher than that of N-MORB (Table 5). The latter possibility was investigated by doubling the Sr content of the model source and repeating the model calculations. The results (circles in Fig. 11b) are more consistent with the adakite data set, but only the 5 and 10 wt% melting models produce Sr/Y ratios within the adakite fields and those results are at or near the bottom of the adakite range. The melting models that produced adakite-like Sr/Y ratios had amphibole-free restites.

The trace element models presented here do not consider interaction between the model slab melts and the mantle wedge during ascent of the magmas to the surface. Without a detailed knowledge of the stoichiometry of the reaction(s) and the melt/mantle ratios, it is not possible to assess quantitatively the effect of that melt/mantle interaction. However, as discussed above, interaction of silicic melts with mantle peridotite consumes olivine, clinopyroxene and spinel and precipitates amphibole and orthopyroxene (Sen and Dunn 1993; Sen 1994). Qualitatively, assimilation of clinopyroxene should decrease the Sr/Y and

Fig. 11a, b Results of the trace element models for batch melting at 2.0 GPa. Data for adakites are from: 1 Adak Island (Kay 1978), 2 Mt. St. Helens (Smith and Leeman 1987), 3 Panama (Defant et al. 1991), 4 Mindanao (Sajona et al. 1993), 5 - Patagonia (Puig et al. 1984) and 6 Baja California (Rogers et al. 1985). **a** Chondrite normalized (Anders and Grevesse 1989) REE patterns for the 2, 5, 10, 15, 20 and 30 percent slab melting models. **b** Plot of Sr/Y versus Y comparing trace element models to adakites. *Filled squares* show the results for the 1, 2, 5, 10, and 15 wt% melting models of N-MORB source. *Open squares* show the result of the 20 and 30 wt% batch melting models. *Filled and open* circles show results of melting models for Sr-enriched N-MORB source

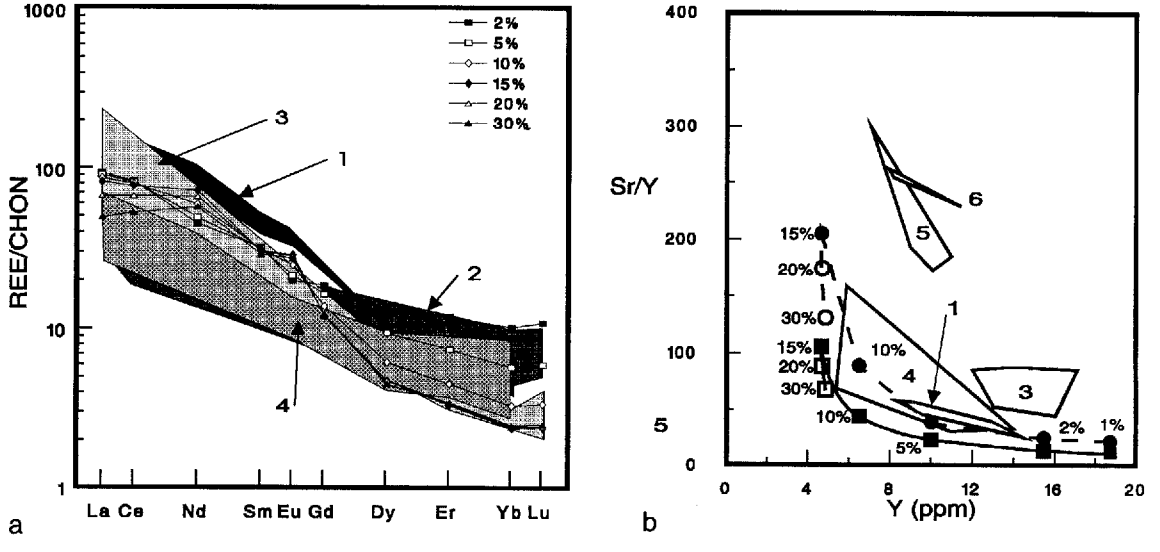

LREE/HREE ratios of the melt. In contrast, while amphibole precipitation should result in an increase in the Sr/Y and LREE/HREE ratios of the melt (D(Sr) < D(Y), Table 5), it will further decrease the Y contents of the melts. The effects of olivine assimilation and orthopyroxene precipitation should approximately cancel for the LREE and Sr, since partition coefficients for those phases are similar (e.g., Dunn and Sen 1994). However, since Y and the HREE are much more compatible in orthopyroxene than in olivine (Dunn and Sen 1994), the effects of melt/mantle interaction will depend on the ratio of olivine assimilation to orthopyroxene precipitation. Overall, the effects may cancel out, or make the trace element systematics either more or less like those of adakites.

The results of the trace element modelling suggest that if adakites are the products of slab melting at approximately 2 GPa, then they must be derived by approximately 15 wt% melting of a source with a significantly higher Sr/Y ratio than N-MORB (i.e., more than twice as high). The models further suggest that the slab restite consists of only garnet and clinopyroxene, not roughly equal proportions of garnet, clinopyroxene and amphibole as suggested by Defant et al. (1991) and Defant and Drummond (1993).

Conclusions

The results show that dehydration melting of amphibolite produces an omphacitic clinopyroxene and garnet bearing residue coexisting with rhyolitic to andesitic composition melts. The experimental results were combined with data from the literature to generate a composite $P - T$ phase diagram for basaltic composition amphibolites over the 800 to 1100° C temperature range for pressures up to 2.0 GPa. Analysis of plots of phase proportions versus melt fraction were used to determine approximate melting reactions at 1.5 and 2.0 GPa. The curves suggest that the amphibolite underwent dehydration melting in two stages, separated by the quartz-out reaction, between 800 and 1025° C at 1.5 GPa. At 2.0 GPa, the original amphibolite minerals reacted out to produce an eclogitic residue coexisting with a melt above 950° C. With further increase in temperature, the eclogite residue began to melt.

Comparison of the major element compositions of the melts with compositions of presumed slab melts (i.e., adakites) shows that partial melting of amphibolite at conditions appropriate to a hot-slab geotherm can generate melts that resemble MgO- and CaO-poor adakites. The experimental results suggest that if adakites are slab melts, then they must gain MgO and CaO during their transit of the mantle wedge.

Trace element models based on the 2.0 GPa melting relations produce adakite-like REE patterns at 10 to 15 wt% melting, but do not reproduce the Sr and Y systematics of adakites. The models require that the Sr/Y ratio of the adakite source be substantially higher than N-MORB, or that the high Sr/Y ratios be acquired after separation of the magmas from the source region.

Taken together, the major and trace element results are not consistent with the derivation of adakites by dehydration melting of the subducted slab with little or no interaction with the mantle wedge or crust. If adakites are partial melts of the subducted slab, then they must undergo significant interaction with the mantle and possibly with the crust, during which they acquire a number of their distinctive characteristics.

Acknowledgements This work was supported by funds from NSERC grants OGP0001893 and EGP0027265 awarded to T. Dunn. C. Sen was supported during part of this study by a scholarship from the Karadeniz Technical University, Trabzon, Turkey. We thank B. Spark for providing the starting amphibolite. This work has benefitted from careful reviews by J.S. Beard, R.J. Stern and an anonymous reviewer.

References

Anders E, Grevesse N (1989) Abundances of the elements:meteoritic and solar. Geochim Cosmochim Acta 53:197–214

Barker F, Arth JG, Stern TW (1986) Evolution of the Coast batholith along the Skagway Traverse, Alaska and British Columbia. Am Mineral 71:632–643

Beard JS, Lofgren GE (1991) Dehydration melting and water saturated melting of basaltic and andesitic greenstones and amphibolites at 1, 3 and 6.9 kb. J Petrol 32:365–401

Defant MJ, Drummond MS (1990) Derivation of some modern arc magmas by melting of young subducted lithosphere. Nature 347:662–665

Defant MJ, Drummond MS (1993) Mount St. Helens:potential example of the partial melting of the subducted lithosphere in a volcanic arc. Geology 21:547–550

Defant MJ, Richerson PM, De Boer JZ, Stewart RH, Maury RC, Bellon H, Drummond MS, Feigenson MD, Jackson TE (1991) Dacite genesis via both slab melting and differentiation:petrogenesis of La Yeguada Volcanic Complex, Panama. J Petrol 32:1143–1167

Drummond MS, Defant MJ (1990) A model for trondhjemite-tonalite-dacite genesis and crustal growth via slab melting:Archean to modern comparisons. J Geophys Res 95:21503–21521

Dunn T, Sen C (1994) Mineral/matrix partition coefficients for orthopyroxene, plagioclase and olivine in basaltic to andesitic systems:a combined analytical and experimental study. Geochim Cosmochim Acta 58:717–733

Gilbert MC, Helz RT, Popp RK, Spear FS (1982) Experimental studies of amphibole stability. In:Veblen DR, Ribbe PH (eds) Amphiboles:petrology and experimental phase relations (Reviews in Mineralogy vol. 9B), Mineralogical Society of America, Washington DC, pp 229–346

Grove TL, Bence AE (1977) Experimental study of pyroxene-liquid interaction in quartz normative basalt. Proc Lunar Sci Conf 8:1549–1579

Haggerty SE (1990) Redox state of continental lithosphere. In:Menzies MA (ed) Continental mantle. Oxford University Press, Oxford, pp 87–102

Hofmann AW (1988) Chemical differentiation of the Earth:the relationship between mantle, continental crust, and oceanic crust. Earth Planet Sci Lett 90:297–314

Holloway JR, Pan V, Gudmundsson G (1992) High-pressure fluid absent melting experiments in the presence of graphite:oxygen fugacity, ferric/ferrous ratio and dissolved CO_2. Eur J Mineral 4:105 114

Johnston AD, Wyllie PJ (1989) The system tonalite-peridotite-H_2O at 30 kbar, with applications to hybridization in subduction zone magmatism. Contrib Mineral Petrol 102:257–264

Kay RW (1978) Aleutian magnesian andesites:melts from subducted Pacific oceanic crust. J Volcanol Geotherm Res 4:117–132

Kay SM, Ramos VA, Marquez M (1993) Evidence in Cerro Pampa volcanic rocks for slab melting prior to ridge-trench collision in southern South America. J Geol 101:703–714

Kress VC, Carmichael ISE (1991) The compressibility of silicate liquids containing Fe_2O_3 and effect of composition, temperature, oxygen fugacity and pressure on their redox states. Contrib Mineral Petrol 108:82–92

Lindsley DH (1983) Pyroxene thermometry. Am Mineral 68:477–493

Martin H (1987) Petrogenesis of Archean trondhjemites, tonalites, and granodiorites from eastern Finland:major and trace element geochemistry. J Petrol 28:921–953

Nicholls JA, Ringwood AE (1973) Effect of water on olivine stability in theoleiites and the production of silica saturated magmas in the island-arc environment. J Geol 81:285–300

Nielsen RL, Drake MJ (1979) Pyroxene-melt equilibria. Geochim Cosmochim Acta 43:1259–1272

Peacock SM (1991) Numerical simulation of subduction zone pressure-temperature-time paths:constraints on fluid production and arc magmatism. Phil Trans R Soc London A335:341–353

Peacock SM (1993) The importance of blueschist to eclogite dehydration reactions in subducting oceanic crust. Geol Soc Am Bull 105:684–694

Puig A, Herve E, Suarez M, Saunders AD (1984) Calc-alkaline and alkaline Miocene and calc-alkaline Recent volcanism in the southernmost Patagonian Cordillera, Chile. J Volcanol Geotherm Res 20:149–163

Rapp RP, Watson EB, Miller CF (1991) Partial melting of amphibolite/eclogite and the origin of Archean trondhjemites and tonalites. Precambrian Res 51:1–25

Rogers G, Saunders AD (1989) Magnesian andesites from Mexico, Chile and the Aleutian Islands:Implications for magmatism associated with ridge-trench collision. In:Crawford AJ (ed) Boninites and related rocks. Unwin Hyman London, pp 417–445

Rogers G, Saunders AD, Terrell DJ, Verma SP, Marriner GF (1985) Geochemistry of Holocene volcanic rocks associated with ridge subduction in Baja, California, Mexico. Nature 315:389–392

Rushmer T (1991) Partial melting of two amphibolites:contrasting experimental results under fluid-absent conditions. Contrib Mineral Petrol 107:41–59

Sajona FG, Maury RC, Bellon H, Cotten J, Defant MJ, Pubellier M (1993) Initiation of subduction and the generation of slab melts in western and eastern Mindanao, Philipines. Geology 21:1007–1010

Sekine T, Wyllie PJ (1982) The system granite-peridotite-H_2O at 30 kbar, with applications to hybridization in subduction zone magmatism. Contrib Mineral Petrol 82:190 202

Sen C (1994) Subduction related petrologic processes:1 - Dehydration melting of a basaltic composition amphibolite, 2 - Mantle metasomatism. PhD Thesis, Univ New Brunswick

Sen C, Dunn T (1993) Experimental production of modally metasomatized mantle. Geol Assoc Can/Mineral Assoc Can Prog Abstr 18:A-95

Smith DR, Leeman WP (1987) Petrogenesis of Mount St. Helens dacitic magmas. J Geophys Res 92:10313–10334

Stolper EM (1982) The speciation of water in silicate melts. Geochim Cosmochim Acta 46:2609–2620

Stolper E, Holloway JR (1988) Experimental determination of the solubility of carbon dioxide in molten basalt at low pressure. Earth Planet Sci Lett 87:397–408

Wolf MB (1992) Amphibolite-tonalite relationships. Part I. Experimental investigation of the phase relationships and textural development of amphibolite dehydration-melting. Part II. The geology, petrology and geochronology of a tonalitic and mafic dike swarm (Southwestern Foothills Terrane, California). PhD Thesis, Calif Inst Tech